International Journal of Statistics and Applied Mathematics 2020; 5(4): 213-228

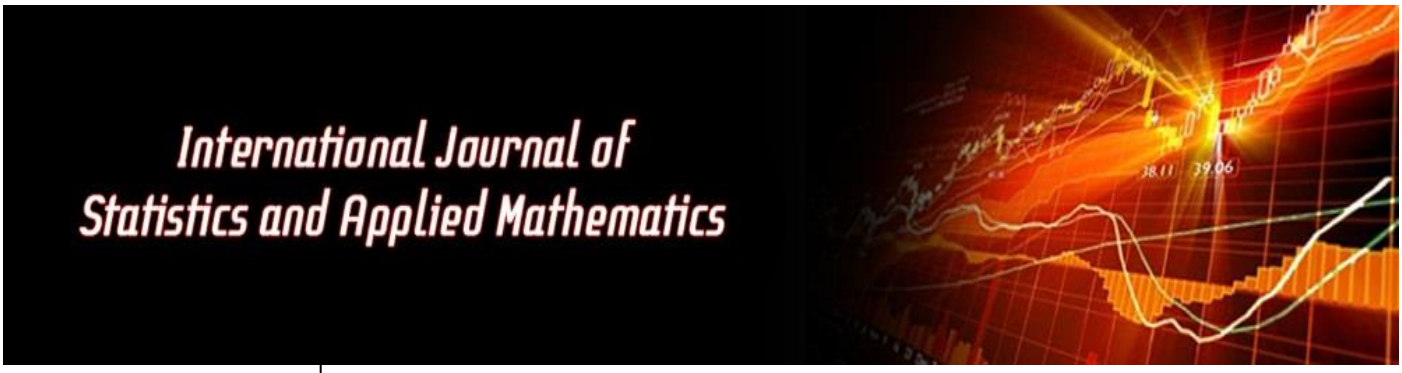

ISSN: 2456-1452
Maths 2020; 5(4): 213-228

www.mathsjournal.com
Received: 20-04-2020
Accepted: 25-05-2020

Sonia Shivhare
Normal School, Sootea,
Biswanath, Assam, India

Corresponding Author:
Sonia Shivhare
Normal School, Sootea,
Biswanath, Assam, India

In presence of thermal radiation through porous medium unsteady MHD Casson fluid flow past an accelerated vertical plate

Dr. Anjan Kumar Deka

Abstract
In this chapter, an attempt has been made to investigate the boundary layer flow of on an unsteady MHD free convection heat and mass transfer flow of a viscous, incompressible and electrically conducting Cassonfluid past an infinite vertical plate embedded in a porous medium. Casson fluid model is used to characterize the fluid behaviour. Heat absorption parameter is incorporated into the equation for the temperature field. The magnetic Reynolds number is considered to be so small that the induced magnetic field can be neglected. Exact solution of the governing equations is obtained in closed form by Laplace transform technique. The expressions for fluid velocity, fluid temperature and species concentration are displayed graphically whereas the numerical values of skin friction, the Nusselt number and the Sherwood number are presented in tabular form for various values of pertinent flow parameters. It is found that the fluid velocity and skin friction are enhanced due to Casson parameters. The fluid velocity and fluid temperature are getting reduced due to heat absorption parameter. Heat absorption parameter has the tendency to reduce the skin friction at the plate. Furthermore, the surface shear stress increases with the increase in the Casson parameter.

Keywords: Nusselt number, skin friction, magnetic field, heat transfer, mass transfer, porous medium, velocity field

Introduction
The study of natural convection flow arises within the fluid when temperature changes cause density variation leading to buoyancy forces which act directly on the fluid elements. Theoretical and experimental study on heat transfer MHD free convection flow with thermal radiation effects on a vertical plate has received deep interest during the last decades. Natural processes such as attenuation of toxic waste in water bodies, vaporization of mist and fog, photosynthesis, transpiration, sea-wind formation, drying of porous solids, and formation of ocean currents [1993] occur due to thermal and solutal buoyancy forces developed as a result of difference in temperature or concentration or a combination of these two. Such configuration is also encountered in several practical systems for industry based applications viz. cooling of molten metals, heat exchanger devices, petroleum reservoirs, insulation systems, filtration, nuclear waste repositories, chemical catalytic reactors and processes, desert coolers, frost formation in vertical channels, wet bulb thermometers, etc. Considering the importance of such fluid flow problems, extensive and in-depth research works have been carried out by several researchers [1971, 1982, 1985, 1988] in the past.
Investigation of hydromagnetic natural convection flow with heat and mass transfer in porous and non-porous media has drawn considerable attentions of several researchers owing to its applications in geophysics, astrophysics, aeronautics, meteorology, electronics, chemical, and metallurgy and petroleum industries. Magneto hydrodynamic (MHD) natural convection flow of an electrically conducting fluid in a fluid with porous medium has also been successfully exploited in crystal formation. Oreper and Szekely [1983] have found that the presence of a magnetic field can suppress natural convection currents and the strength of magnetic field is one of the important factors in reducing non-uniform composition thereby enhancing quality of the crystal. In addition to it, the thermal physics of hydromagnetic problems with mass transfer is of much significance in MHD flow-meters, MHD energy generators, MHD pumps,

controlled thermo-nuclear reactors, MHD accelerators, etc. Keeping in view the importance of such study, Hossain and Mandal [1985] investigated mass transfer effects on unsteady hydromagnetic free convection flow past an accelerated vertical porous plate. Jha [1991] studied hydromagnetic free convection and mass transfer flow past a uniformly accelerated vertical plate through a porous medium when magnetic field is fixed with the moving plate. Chen [2004] analyzed combined heat and mass transfer in MHD free convection flow from a vertical surface with Ohmic heating and viscous dissipation. Chamkha [2004] investigated unsteady MHD convection flow with heat and mass transfer past a semi-infinite vertical permeable moving plate in a uniform porous medium with heat absorption.

In recent years non-Newtonian fluids have outspread applications in chemical, cosmetic and pharmaceutical industries such as in the production of several chemicals, gas, paint, oil, syrup, juice, deodorizer and cleanser [1989]. In Newtonian fluid the viscous stresses arising from its flow, at every point are linearly proportional to the local strain rate and they have limited applications. They cannot describe various facts noticed for the fluids in industrial and other technological applications such as soap, certain oils, paints, blood and many emulsions. It is well known that the mechanics of non-Newtonian fluids present a special challenge to engineers, mathematicians and physicists. Navier-Stokes' equations are not able to describe the properties of such fluids and no single constitutive equation is accessible which exhibits the properties of all fluids. Rheological properties of non-Newtonian fluids are described by their constitutive equations In the earlier studies on Casson fluid, Fredrickson [1964] investigated its steady flow in a tube. Mernone *et al*. [2002] described the peristaltic flow of a Casson fluid in a two dimensional channel. Boyd *et al*. [2007] described the steady and oscillatory flow of blood flow by taking into account Casson fluid model. Mukhopadhyay [2013] described the effects of thermal radiation on Casson fluid flow and heat transfer over an unsteady stretching surface. Mustafa *et al*. [2011] studied boundary layer flow and heat transfer of a Casson fluid over a moving flat plate with a parallel free stream using homotopy analysis model (HAM). Hayat *et al*. [2012] examined the mixed convection stagnation point flow of Casson fluid with convective boundary conditions. Pramanik [2014] studied the Casson fluid flow and heat transfer past an exponential porous stretching surface in the presence of thermal radiation. Bhattacharyya [2013] investigated the boundary layer stagnation point flow of Casson fluid and heat transfer towards a shrinking/stretching sheet. Animasaun *et al*. [2013] studied Casson fluid flow with variable thermo-physical property along exponentially stretching sheet with suction and exponentially decaying internal heat generation using the homotopy analysis method (HAM). Ramachandra Prasad *et al*. [2013] analyzed the Flow and Heat Transfer of Casson Fluid from a horizontal circular cylinder with partial slip in non-Darcy porous medium. The heat transfer aspects of the Casson fluid flow is an important research area due to its relevance to the optimized processing of chocolate, toffee and other foodstuffs [2002]. Recently, Das *et al*. [2015] studied the effect of Newtonian heating on an unsteady hydromagnetic Casson fluid flow past a flat plate with heat and mass transfer. Akbar and Khan [2015] studied the metachronal beating of cilia under the influence of magnetic field on peristaltic flow of a Casson fluid in an asymmetric channel an application in crude oil refinement. Physiological transportation of Casson fluid in a plumb duct was investigated by Akbar and Butt [2015].

The purpose of present study is to analyze the effect of thermal radiation and heat absorption parameter on an unsteady MHD free convection flow of a viscous, incompressible, electrically conducting Casson fluid past an impulsively moving vertical plate in a porous medium. The governing equations are first transformed into a set of normalized equations and then solved analytically by using Laplace transform technique and a general solution is obtained. The effects of different involved parameters such as magnetic field parameter, Schmidt number, Prandtl number, Grash of number for heat transfer and mass transfer, chemical reaction, thermal radiation, heat absorption parameter and Casson parameter on the fluid velocity, temperature and concentration distributions are plotted and discussed.

Mathematical Analysis: Consider the unsteady MHD natural convection flow with heat and mass transfer of a viscous, incompressible, electrically conducting, heat absorption and chemically reactive Casson fluid along an infinite vertical plate embedded in a uniform porous medium.

Coordinate system is chosen in such a way that x'-axis is considered along the plate in upward direction and y'-axis normal to plane of the plate in the fluid. A uniform transverse magnetic field B_0 is applied in a direction which is parallel to y'-axis. Initially i.e., at time $t' \le 0$, both the fluid and plate are at rest and are maintained at a uniform temperature T'_∞. Also species concentration at the surface of the plate as well as at every point within the fluid is maintained at uniform concentration C'_∞. At time $t' > 0$, plate starts moving in x' - direction with a velocity $u' = Ut'$ in its own plane. The temperature at the surface of the plate is raised to uniform temperature T'_w and species concentration at the surface of the plate is raised to uniform species concentration C'_w and is maintained thereafter. Geometry of the problem is presented in Fig.3.1. Since plate is of infinite extent in x' and z' directions and is electrically non-conducting, all physical quantities except pressure depend on y' and t' only. Also no applied or polarized voltages exist so the effect of polarization of fluid is negligible. This corresponds to the case where no energy is added or extracted from the fluid by electrical means [1973]. It is assumed that the induced magnetic field generated by fluid motion is negligible in comparison to the applied one.

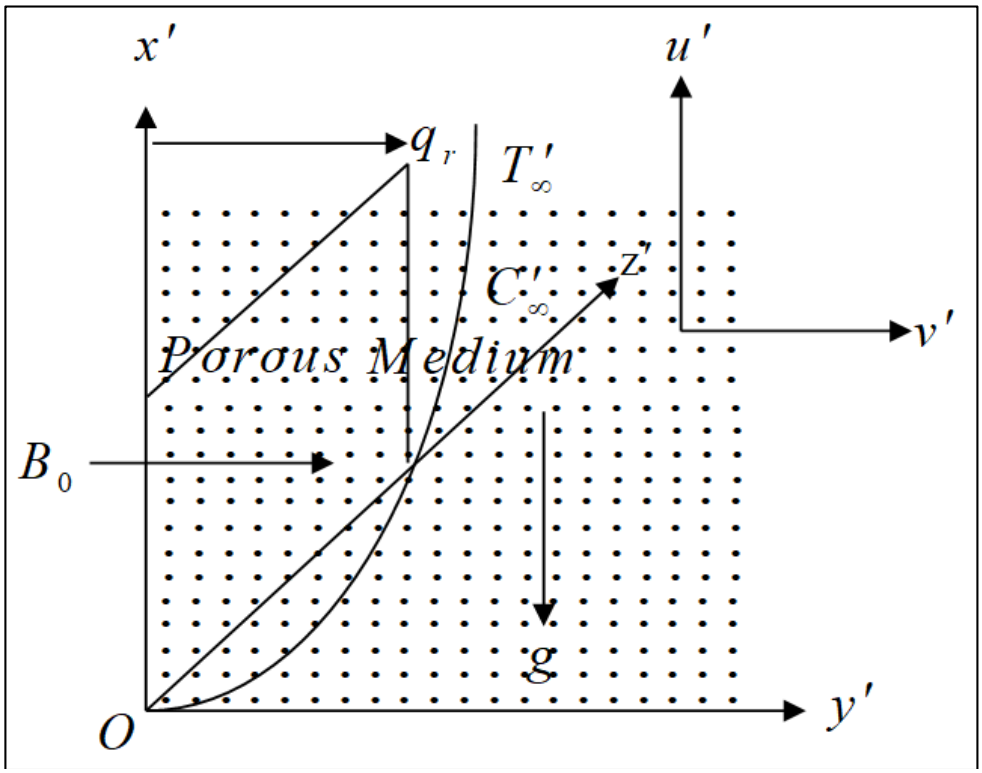

Fig 3.1: Geometry of the Problem

This assumption is justified because magnetic Reynolds number is very small for liquid metals and partially ionized fluids which are commonly used in industrial applications [1973]. Assuming the rheological equation for an incompressible and isotropic Casson fluid represented by Casson [1959] is

$$\tau = \tau_0 + \mu\alpha^*$$

equivalently,

$$\tau_{ij} = \begin{cases} 2\left(\mu_B + \frac{p_y}{\sqrt{2\pi}}\right)e_{ij}, \pi > \pi_c \\ 2\left(\mu_B + \frac{p_y}{\sqrt{2\pi_c}}\right)e_{ij}, \pi < \pi_c \end{cases}$$

where τ, τ_0, μ and α^* are, respectively shear stress, Casson yield stress, dynamic viscosity and shear rate and $\pi = e_{ij}e_{ij}$ and e_{ij} is the (i, j)thcomponent of deformation rate, π is the product based on the non-Newtonian fluid, π_c is a critical value of this product, μ_B is the plastic dynamic viscosity of the non-Newtonian fluid, and p_y denote the yield stress of the fluid.
Keeping in view the assumptions made above, governing equations for the fully developed hydromagnetic natural convection flow with heat and mass transfer of an electrically conducting, viscous, incompressible, heat absorbing and chemically reactive Cassonfluid past an infinite vertical plate embedded in a uniform porous medium are

Conservation of momentum

$$\frac{\partial u'}{\partial t'} = \upsilon\left(1+\frac{1}{\alpha}\right)\frac{\partial^2 u'}{\partial y^{2'}} + g\beta\left(T'-T'_\infty\right) + g\beta'\left(C'-C'_\infty\right) - \frac{\sigma B_0^2}{\rho}u' - \frac{\upsilon}{K'_1}u' \quad (3.2.1)$$

Conservation of energy

$$\frac{\partial T'}{\partial t'} = \frac{k}{\rho Cp}\frac{\partial^2 T'}{\partial y^{2'}} - \frac{1}{\rho Cp}\frac{\partial q'_r}{\partial y'} - \frac{Q_0}{\rho Cp}\left(T'-T'_\infty\right) \quad (3.2.2)$$

Conservation of species concentration

$$\frac{\partial C'}{\partial t'} = D\frac{\partial^2 C'}{\partial y'^2} - Kr'\left(C' - C'_\infty\right) \tag{3.2.3}$$

where $u', g, \alpha, \rho, \beta, \beta', k, C_p, \sigma, \upsilon, D, T', C', Kr', q'_r$ and K'_1 are, respectively, the fluid velocity in the x' -direction, acceleration due to gravity, Casson fluid parameter, the fluid density, the volumetric coefficient of thermal expansion, the volumetric coefficient of expansion for concentration, thermal conductivity, specific heat at constant pressure, electrical conductivity, the kinematic viscosity, the coefficient of mass diffusivity, the temperature of the fluid, species concentration, chemical reaction parameter, radiative heat flux vector and permeability of the porous medium.
Initial and boundary conditions for the fluid flow problem are given below:

$$u' = 0, T' = T'_\infty, C' = C'_\infty \text{ for all } y' \text{ and } t' \le 0 \tag{3.2.4a}$$

$$u' = Ut', T' = T'_w, C' = C'_w \text{ at } y' = 0 \text{ for } t' > 0 \tag{3.2.4b}$$

$$u' \to 0, T' \to T'_\infty, C' \to C'_\infty \text{ as } y' \to \infty \text{ for } t' > 0 \tag{3.2.4c}$$

For an optically thick fluid, in addition to emission there is also self absorption and usually the absorption co-efficient is wavelength dependent and large so we can adopt the Rosseland approximation for radiative heat flux vector q_r'. Thus q_r' is given by

$$q_r' = -\frac{4\sigma_1}{3k_1}\frac{\partial T'^4}{\partial y'} \tag{3.2.5}$$

where k_1 is Rosseland mean absorption co-efficient and σ_1 is Stefan-Boltzmann constant.
We assume that the temperature differences within the flow is sufficiently small, then equation (3.2.5) can be linearized by expanding T'^4 into Taylor's series about the free stream temperature T_∞' and neglecting second and higher order terms in $\left(T' - T'_\infty\right)$. This results of the following approximations:

$$T'^4 \approx 4T'^3_\infty T' - 3T'^4_\infty \tag{3.2.6}$$

From (3.2.5) and (3.2.6) we have

$$\frac{\partial q_r'}{\partial y'} = -\frac{4\sigma_1}{3k_1}\frac{\partial^2 T'^4}{\partial y'^2} = -\frac{16\sigma_1 T'^3_\infty}{3k_1}\frac{\partial^2 T'}{\partial y'^2} \tag{3.2.7}$$

Thus the energy equation (3.2.3) reduces to

$$\frac{\partial T'}{\partial t'} = \frac{k}{\rho C_p}\frac{\partial^2 T'}{\partial y'^2} - \frac{Q_0}{\rho C_p}\left(T' - T'_\infty\right) + \frac{16\sigma_1 T'^3_\infty}{3k_1\rho C_p}\frac{\partial^2 T'}{\partial y'^2} \tag{3.2.8}$$

In order to reduce the governing equations (3.2.1), (3.2.3) and (3.2.8), into non-dimensional form, the following dimensionless variables and parameters are introduced.

$$y = \frac{y'U_0}{\upsilon}, u = \frac{u'}{U_0}, U = \frac{U_0^3}{\upsilon}, t = \frac{t'U_0^2}{\upsilon}, T = \frac{T' - T'_\infty}{T'_w - T'_\infty}, C = \frac{C' - C'_\infty}{C'_w - C'_\infty}, Gr = \frac{g\beta\upsilon\left(T'_w - T'\right)}{U_0^3},$$

$$Gm = \frac{g\beta'\upsilon\left(C'_w - C'_\infty\right)}{U_0^3}, M = \frac{\sigma B_0^2\upsilon}{\rho U_0^2}, Pr = \frac{\mu Cp}{k}, Sc = \frac{\upsilon}{D}, Q = \frac{\upsilon Q_0}{\rho CpU_0^2}, K_1 = \frac{K'_1U_0^2}{\upsilon^2},$$

$$N=\frac{kk_1}{4\sigma_1 T_\infty'^3},\lambda=\frac{3N+4}{3N},Kr=\frac{\upsilon Kr'}{U_0^2}.$$

where Gr, Gm, M, Pr, Sc, Q and N are, respectively, the thermal Grashof number, the solutal Grashof number, the magnetic parameter, the Prandtl number, the Schmidt number, the heat absorption parameter and radiation parameter.
Equation (3.2.1), (3.2.3) and (3.2.8) reduces to

$$\frac{\partial u}{\partial t}=\left(1+\frac{1}{\alpha}\right)\frac{\partial^2 u}{\partial y^2}+GrT+GmC-Mu-\frac{u}{K_1} \quad (3.2.9)$$

$$\frac{\partial T}{\partial t}=\frac{\lambda}{Pr}\frac{\partial^2 T}{\partial y^2}-QT \quad (3.2.10)$$

$$\frac{\partial C}{\partial t}=\frac{1}{Sc}\frac{\partial^2 C}{\partial y^2}-KrC \quad (3.2.11)$$

The corresponding initial and boundary conditions in non-dimensional form become:

$$u=0,\theta=0,\phi=0 \text{ for all y and } t\le 0 \quad (3.2.12a)$$

$$u=t,T=1,C=1 \text{ at } y=0 \text{ for } t>0 \quad (3.2.12b)$$

$$u\to 0,T\to 0,C\to 0 \text{ as } y\to\infty \text{ for } t>0 \quad (3.2.12c)$$

Method of Solutions

The set of equations (3.2.9), (3.2.10) and (3.2.11) subject to the initial and boundary conditions (3.2.12a)-(3.2.12c) were solved analytically using Laplace transforms. The exact solutions for fluid velocity $u(y,t)$, fluid temperature $T(y,t)$ and species concentration $C(y,t)$ are obtained and expressed in the following form:

$$u(y,t)=\frac{1}{2}\left[\left(t+\frac{y}{2\sqrt{A_1A_2}}\right)e^{y\sqrt{A_2/A_1}}\operatorname{erfc}\left(\frac{y}{2\sqrt{A_1t}}+\sqrt{A_2t}\right)+\left(t-\frac{y}{2\sqrt{A_1A_2}}\right)e^{-y\sqrt{A_2/A_1}}\operatorname{erfc}\left(\frac{y}{2\sqrt{A_1t}}-\sqrt{A_2t}\right)\right]+$$

$$\frac{A_9}{2}e^{A_7t}\left\{e^{y\sqrt{(A_2+A_7)/A_1}}\operatorname{erfc}\left(\frac{y}{2\sqrt{A_1t}}+\sqrt{(A_2+A_7)t}\right)+e^{-y\sqrt{(A_2+A_7)/A_1}}\operatorname{erfc}\left(\frac{y}{2\sqrt{A_1t}}-\sqrt{(A_2+A_7)t}\right)\right\}+$$

$$\frac{A_{10}}{2}e^{A_8t}\left\{e^{y\sqrt{(A_2+A_8)/A_1}}\operatorname{erfc}\left(\frac{y}{2\sqrt{A_1t}}+\sqrt{(A_2+A_8)t}\right)+e^{-y\sqrt{(A_2+A_8)/A_1}}\operatorname{erfc}\left(\frac{y}{2\sqrt{A_1t}}-\sqrt{(A_2+A_8)t}\right)\right\}-$$

$$\frac{1}{2}(A_9+A_{10})\left\{e^{y\sqrt{A_2/A_1}}\operatorname{erfc}\left(\frac{y}{2\sqrt{A_1t}}+\sqrt{A_2t}\right)+e^{-y\sqrt{A_2/A_1}}\operatorname{erfc}\left(\frac{y}{2\sqrt{A_1t}}-\sqrt{A_2t}\right)\right\}-$$

$$\frac{A_9}{2}e^{A_7t}\left\{e^{y\sqrt{\frac{Pr}{\lambda}(A_7+Q)}}\operatorname{erfc}\left(\frac{y}{2}\sqrt{\frac{Pr}{\lambda t}}+\sqrt{(A_7+Q)t}\right)+e^{-y\sqrt{\frac{Pr}{\lambda}(A_7+Q)}}\operatorname{erfc}\left(\frac{y}{2}\sqrt{\frac{Pr}{\lambda t}}-\sqrt{(A_7+Q)t}\right)\right\}+$$

$$\frac{A_9}{2}\left\{e^{y\sqrt{\frac{PrQ}{\lambda}}}\operatorname{erfc}\left(\frac{y}{2}\sqrt{\frac{Pr}{\lambda t}}+\sqrt{Qt}\right)+e^{-y\sqrt{\frac{PrQ}{\lambda}}}\operatorname{erfc}\left(\frac{y}{2}\sqrt{\frac{Pr}{\lambda t}}-\sqrt{Qt}\right)\right\}-$$

$$\frac{A_{10}}{2}e^{A_8 t}\left\{e^{y\sqrt{Sc(A_8+Kr)}}erfc\left(\frac{y}{2}\sqrt{\frac{Sc}{t}}+\sqrt{(A_8+Kr)t}\right)+e^{-y\sqrt{Sc(A_8+Kr)}}erfc\left(\frac{y}{2}\sqrt{\frac{Sc}{t}}-\sqrt{(A_8+Kr)t}\right)\right\}+$$

$$\frac{A_{10}}{2}\left\{e^{y\sqrt{ScKr}}erfc\left(\frac{y}{2}\sqrt{\frac{Sc}{t}}+\sqrt{Krt}\right)+e^{-y\sqrt{ScKr}}erfc\left(\frac{y}{2}\sqrt{\frac{Sc}{t}}-\sqrt{Krt}\right)\right\} \quad (3.3.1)$$

$$T(y,t)=\frac{1}{2}\left\{e^{y\sqrt{\frac{PrQ}{\lambda}}}erfc\left(\frac{y}{2}\sqrt{\frac{Pr}{\lambda t}}+\sqrt{Qt}\right)+e^{-y\sqrt{\frac{PrQ}{\lambda}}}erfc\left(\frac{y}{2}\sqrt{\frac{Pr}{\lambda t}}-\sqrt{Qt}\right)\right\} \quad (3.3.2)$$

$$C(y,t)=\frac{1}{2}\left\{e^{y\sqrt{ScKr}}erfc\left(\frac{y}{2}\sqrt{\frac{Sc}{t}}+\sqrt{Krt}\right)+e^{-y\sqrt{ScKr}}erfc\left(\frac{y}{2}\sqrt{\frac{Sc}{t}}-\sqrt{Krt}\right)\right\} \quad (3.3.3)$$

Skin-Friction, The rate of heat transfer and the rate of mass transfer

The expression for the skin friction at the plate, is given by

$$\tau=\left(\frac{\partial u}{\partial y}\right)_{y=0}=-\left\{\frac{1}{2\sqrt{A_1A_2}}erf\left(\sqrt{A_2 t}\right)+t\sqrt{\frac{A_2}{A_1}}erf\left(\sqrt{A_2 t}\right)+\sqrt{\frac{t}{A_1\pi}}e^{-A_2 t}\right\}+$$

$$A_9 e^{A_7 t}\left\{\sqrt{\frac{Pr}{\lambda}(A_7+Q)}erf\left(\sqrt{(A_7+Q)t}\right)-\sqrt{(A_2+A_7)/A_1}erf\left(\sqrt{(A_2+A_7)t}\right)+\sqrt{\frac{Pr}{\pi\lambda t}}e^{-(A_7+Q)t}-\frac{e^{-(A_2+A_7)t}}{\sqrt{A_1\pi t}}\right\}+$$

$$A_{10}e^{A_8 t}\left\{\sqrt{Sc(A_8+Kr)}erf\left(\sqrt{(A_8+Kr)t}\right)-\sqrt{(A_2+A_8)/A_1}erf\left(\sqrt{(A_2+A_8)t}\right)+\sqrt{\frac{Sc}{\pi t}}e^{-(A_8+Kr)t}-\frac{e^{-(A_2+A_8)t}}{\sqrt{A_1\pi t}}\right\}+$$

$$A_9\left\{\sqrt{\frac{A_2}{A_1}}erf\left(\sqrt{A_2 t}\right)-\sqrt{\frac{PrQ}{\lambda}}erf\left(\sqrt{Qt}\right)+\frac{e^{-A_2 t}}{\sqrt{A_1\pi t}}-\sqrt{\frac{Pr}{\pi\lambda t}}e^{-Qt}\right\}+$$

$$A_{10}\left\{\sqrt{\frac{A_2}{A_1}}erf\left(\sqrt{A_2 t}\right)-\sqrt{ScKr}erf\left(\sqrt{Krt}\right)+\frac{e^{-A_2 t}}{\sqrt{A_1\pi t}}-\sqrt{\frac{Sc}{\pi t}}e^{-Krt}\right\} \quad (3.4.1)$$

The Nusselt number Nu, which measures the rate of heat transfer at the plate, is given by

$$Nu=-\left(\frac{\partial T}{\partial y}\right)_{y=0}=\sqrt{\frac{PrQ}{\lambda}}erf\left(\sqrt{Qt}\right)+\sqrt{\frac{Pr}{\pi\lambda t}}e^{-Qt} \quad (3.4.2)$$

The Sherwood number Sh, which measures the rate of mass transfer at the plate, is given by

$$Sh=-\left(\frac{\partial C}{\partial y}\right)_{y=0}=\sqrt{ScKr}erf\left(\sqrt{Krt}\right)+\sqrt{\frac{Sc}{\pi t}}e^{-Krt} \quad (3.4.3)$$

Results and Discussions: In order to get the physical understand of the considered problem and for the purpose of analyzing the effect of Casson parameter (α), thermal Grashof number (Gr), solutalGrashof number (Gm), Magnetic parameter (M), Prandtl number (Pr), thermal radiation parameter (N), Schmidt number (Sc), chemical reaction parameter (Kr) and time (t) on the flow field, numerical values of the fluid velocity, fluid temperature and species concentration in the boundary layer region were computed and are displayed graphically versus boundary layer co-ordinate y in Figs 3.2-3.19. The numerical values of skin friction, heat transfer co-efficient in terms of Nusselt number (Nu) and mass transfer co-efficient in terms of Sherwood number (Sh) are depicted in Tables 3.1-3.9. During the course of numerical calculations of the fluid velocity, the temperature and the

species concentration, the values of the Prandtl number are chosen for air at 25^0C and one atmospheric pressure (Pr=0.71), electrolytic solution (Pr=1.0), water (Pr=7.0) and water at 4^0C (Pr=11.62). To focus our attention on numerical values of the results obtained in the study, the values of Sc are chosen for the gases representing diffusing chemical species of most common interest in air, namely, hydrogen (Sc=0.22), water-vapour (Sc=0.60), ammonia (Sc=0.78) and methanol (Sc=1.0). To examine the effect of parameters related to the problem on the velocity field, the skin friction numerical computation are carried out at Pr=0.71 and Sc=0.22. To find solution of this problem, we have placed an infinite vertical plate in a finite length in the flow. Hence, we solve the entire problem in a finite boundary.

Figs.3.2-3.3 depicts the influence of thermal and concentration buoyancy forces on fluid velocity. It is perceived from Figs.3.2-3.3 that the fluid velocity increases on increasing values of Gr and Gm throughout the boundary layer region. Gr represents the relative strength of thermal buoyancy force to viscous force and Gm represents the relative strength of concentration buoyancy force to viscous force. Therefore, Gr increases on increasing the strengths of thermal buoyancy force whereas Gm increases on increasing the strength of concentration buoyancy force. In this problem, natural convection flow induced due to thermal and concentration buoyancy forces; therefore, thermal and concentration buoyancy force tends to accelerate the fluid velocity throughout the boundary layer region which is clearly evident from Figs.3.2-3.3.

Effect of Casson parameter α on velocity profile is clearly exhibited in Fig.3.4. It is observed that the fluid velocity increases close to the boundary of the wall with increasing values of α. The effect of increasing values of α is to increase the fluid velocity, and hence the boundary layer thickness increases. The increasing values of the Casson parameter i.e., the decreasing yield stress (the fluid behaves as Newtonian fluid as Casson parameter becomes large i.e., for $\alpha \to \infty, \frac{1}{\alpha} \to 0$) increases the velocity field. It can also be seen from Fig.3.4 that the momentum boundary layer thickness increases as α increases and hence induces a decrease in the absolute value of the velocity gradient at the surface.

Fig.3.5 depicts the effect of magnetic field parameter (M) on the velocity field. It is evident from the figure that an increase in the values of magnetic parameter reduces the velocity boundary layer. This is due to the fact that an increase in magnetic field develops the opposite force to the flow direction, which is called Lorentz force and it has the tendency to reduce the boundary layer thickness.

The influence of Schmidt number (Sc) on the fluid velocity and concentration profiles are depicted in Figs.3.6 and 3.7 respectively. It is noticed from Figs.3.6 and 3.7 that, fluid velocity and concentration profiles decreases on increasing the values of Sc. The Schmidt number embodies the ratio of the momentum to the mass diffusivity. The Schmidt number therefore quantifies the relative effectiveness of momentum to mass transport by diffusion in the hydrodynamic (velocity) and concentration (species) boundary layers. As the Schmidt number increases the concentration decreases. This cause the concentration buoyancy effects to decrease yielding a reduction in the fluid velocity. The reductions in the velocity and concentration profiles are accompanied by simultaneous reductions in the velocity and concentration boundary layers. These behaviours are clear from Figs.3.6 and 3.7.

Fig.3.8 depicts the effect of chemical reaction parameter (Kr) on the fluid velocity. As can be seen, an increase in the chemical reaction parameter (Kr) leads to decrease in the thickness of the velocity boundary layer; this shows that diffusion rate can be tremendously altered by chemical reaction. It should be mentioned here that physically positive values of Kr implies destructive reaction and negative values of Kr implies generative reaction. We studied the case of a destructive chemical reaction.

Figs.3.9 and 3.10 demonstrate the influence of thermal radiation parameter (N) on fluid velocity and fluid temperature respectively. It is evident from Figs.3.9 and 3.10 that, the thermal radiation leads to decrease the fluid velocity and fluid temperature. Physically, thermal radiation causes a fall in temperature of fluid medium and thereby causes a fall in kinetic energy of the fluid particles. This results in a corresponding decrease in the fluid velocity. Thus Figs. 3.9 and 3.10 are in excellent agreement with the laws of Physics.

Fig.3.11 illustrates the effect of permeability of porous medium (K_1) on fluid velocity. It is perceived from Fig.3.11 that fluid velocity increases on increasing permeability parameter. From the flow configuration it is obvious that an increase in porosity of the medium assists the flow along the flow direction causing the fluid velocity to increase due to its orientation through the porous medium.

Figs.3.12 and 3.13 present the effect of Prandtl number (Pr) on the fluid velocity and temperature profiles. Prandtl number embodies the ratio of viscous diffusion to thermal diffusion in the boundary layer regime. It also expresses the ratio of the product of specific heat capacity and dynamic viscosity, to the fluid thermal conductivity. When Pr high, viscous diffusion rate is exceeds thermal diffusion rate. An increase in Pr from 0.7 through 1.0, 7.0 to11.42 is found to significantly depress velocities (Fig.3.12) and this trend is sustained throughout the regime. For Pr<1, thermal diffusivity exceeds momentum diffusivity i.e. heat will diffuse faster than momentum. Therefore for lower Pr fluids (e.g.,Pr=0.71), the flow will be accelerates whereas for greater Pr fluids (e.g.Pr=1) it will be strongly decelerated. For Pr=1.0, both the viscous and energy diffusion rates will be the same as will the thermal and velocity boundary layer thicknesses. This case can be representative of food stuffs e.g. low-density polymorphic forms of chocolate suspensions, as noted by Steffe [2011] and Debaste *et al*. [2007]. Temperature is found to be strongly reduced with increasing Prandtl number. For larger Pr values, the decay is found to be increasingly monotonic. Therefore for lower thermal conductivity fluids (as typified by liquid chocolate and other foodstuffs), lower temperatures are observed throughout the boundary layer regime.

Figs.3.14 and 3.15 illustrates the influence of heat absorption parameter (Q) on fluid velocity and fluid temperature respectively. It is evident from Figs.3.14 and 3.15 that as Q increases the pack value of fluid velocity and fluid temperature tends to decrease. Physically, the presence of heat absorption coefficient has the tendency to reduce the fluid temperature. This cause the thermal buoyancy effects to decrease resulting in a net reduction in the fluid velocity.

Fig.3.16 shows the influence of a chemical reaction on concentration profiles. In this study, we are analyzing the effects of a destructive chemical reaction (Kr>0). It is noticed that concentration distributions decrease when the chemical reaction increase. Physically, for a destructive case, chemical reaction takes place with many disturbances. This, in turn, causes high molecular

motion, which results in an increase in the transport phenomenon, thereby reducing the concentration distributions in the fluid flow.

Figs.3.17, 3.18 and 3.19 illustrate the influence of time on fluid velocity, fluid temperature and species concentration respectively. It is evident from Figs.3.17, 3.18 and 3.19 that, the fluid velocity, fluid temperature and species concentration are getting accelerated with the progress of time throughout the boundary layer region. Also it may be noted that, unabated mass diffusion into the fluid stream, the molar concentration of the mixture rises with increasing time and so there is an enhancement in species concentration with the progress of time throughout the boundary layer region.

The numerical values of the skin friction τ, computed from the analytical expression (3.4.1), is presented in tabular form for various values of Gr, Gm, Kr, N, Pr, Sc, Q, α, K_1 and t in Tables 3.1-3.5. It is evident from Tables 3.1-3.5 that, the skin friction increases on increasing Gr, Gm, α and K_1 whereas it decreases on increasing Kr, N, Pr, Sc, Q and t. This implies that, thermal buoyancy force, concentration buoyancy force, Casson parameter and permeability of the porous medium have the tendency to enhance the skin friction coefficient whereas chemical reaction, thermal radiation, Prandtl number, mass diffusion, heat absorption and time has the tendency to reduce the skin friction coefficient at the plate.

The numerical values of heat transfer coefficient in terms of Nusselt number (Nu), computed from the analytical expression (3.4.2), and are presented in tabular form for various values of Pr, Q, N and t in Tables 3.6-3.7. It is noticed from Tables 3.6 and 3.7 that, Nusselt number increases on increasing Prandtl number, heat absorption and thermal radiation whereas it decrease on increasing time. This implies that, thermal diffusion, thermal radiation and heat absorption parameter tend to enhance rate of heat transfer at the plate. As time progress, the rate of heat transfer getting reduced at the plate.

The numerical values of mass transfer coefficient in terms of Sherwood number (Sh), computed from the analytical expression (3.4.3), and are presented in tabular form for various values of Sc, Kr and t in Tables 3.8-3.9. It is revealed from Tables 3.8 and 3.9 that, the rate of mass transfer increases on increasing Sc and Kr whereas it decreases on increasing t. This implies that mass diffusion and chemical reaction parameter tend to enhance the rate of mass transfer at the plate. As time progress, it is noticed that the rate of mass transfer getting reduced at the plate.

Conclusions

The unsteady MHD natural convection flow with heat and mass transfer of a viscous, incompressible, electrically conducting, heat absorption and chemically reactive Casson fluid along an infinite vertical plate embedded in a uniform porous mediumis carried out. Exact solutions of the governing equations were obtained using Laplace transform technique. A comprehensive set of graphical for the fluid velocity, fluid temperature and species concentration is presented and their dependence on some physical parameters is discussed. Significant finding are as follows:

- Momentum boundary layer thickness increases with increasing Casson parameters.
- Heat absorption parameter has the tendency to reduce the fluid velocity and fluid temperature throughout the boundary layer region.
- With increasing Prandtl number, temperature decreases and an increase in Prandtl number reduces the thermal boundary layer thickness.
- Mass diffusion tends to reduce the species concentration and there is an enhancement in species concentration with the progress of time throughout the boundary layer region.
- The surface shear stress increases with the increase in the Casson parameter.
- Thermal diffusion and thermal radiation tend to retard the fluid temperature and there is an enhancement in fluid temperature with the progress of time throughout the boundary layer region.
- Heat absorption parameter has the tendency to reduce the skin friction at the plate.
- Heat absorption parameter tends to enhance the rate of heat transfer whereas as time progress the rate of heat transfer is getting reduced.
- Mass diffusion tends to enhance the rate of mass transfer whereas as time progress the rate of mass transfer is getting reduced.

Tables

Table 3.1: Skin Friction when M=10,Pr=0.71, Sc=0.22, K_1=1, Kr=1, N=1, Q=1, α=1, t=0.5.

Gr↓Gm→	τ			
	5	**10**	**15**	**20**
5	0.6248	1.5826	2.5404	3.4982
10	1.5710	2.5288	3.4866	4.4444
15	2.5172	3.4750	4.4328	5.3906
20	3.4634	4.4212	5.3790	6.3368

Table 3.2: Skin Friction when Gr=5,Gm=5,M=10,Pr=0.71,Sc=0.22, K_1=1, Q=1, α=1, t=0.5.

Kr↓N→	τ			
	1	3	5	7
1	0.6248	0.6092	0.6058	0.6044
3	0.4926	0.4770	0.4736	0.4722
5	0.4175	0.4019	0.3985	0.3971
7	0.3692	0.3536	0.3502	0.3487

Table 3.3: Skin Friction when Gr=5, Gm=5, M=10, K_1=1, Kr=1, N=1, Q=1, α=1, t=0.5.

Pr↓Sc→	τ			
	0.22	**0.6**	**0.78**	**1**
0.71	0.6248	0.4062	0.3745	0.3431
1	0.6133	0.3947	0.3630	0.3316
7	0.2040	-0.0147	-0.0464	-0.0777
11.62	-1.5461	-1.7648	-1.7965	-1.8278

Table 3.4: Skin Friction when Gr=5,Gm=5,M=10,Pr=0.71,Sc=0.22,K_1=1,Kr=1, N=1, t=0.5.

Q↓α→	τ			
	0.5	**1**	**2**	**5**
1	0.4874	0.6248	0.7451	0.8533
3	0.3536	0.4782	0.5906	0.6931
5	0.2781	0.3955	0.5029	0.6016
7	0.2307	0.3429	0.4466	0.5422

Table 3.5: Skin Friction when Gr=5,Gm=5,M=10,Pr=0.71, Sc=0.22, Kr=1, N=1, Q=1, α=1.

K_1↓t→	τ			
	0.5	**1**	**1.5**	**2**
0.5	0.5029	-0.7919	-2.0496	-3.2912
1	0.6248	-0.6238	-1.8325	-3.0235
1.5	0.6680	-0.5649	-1.7568	-2.9305
2	0.6900	-0.5348	-1.7183	-2.8833

Table 3.6: Nusselt Number when N=1, t=0.5.

Pr↓Q→	**Nu**			
	1	**3**	**5**	**7**
0.71	0.6435	0.9741	1.2383	1.4608
1	0.7637	1.1560	1.4696	1.7337
7	2.0207	3.0586	3.8883	4.5870
11.62	2.6034	3.9407	5.0097	5.9099

Table 3.7: Nusselt Number when Pr=0.71, Q=1.

N↓t→	**Nu**			
	0.5	**1**	**1.5**	**2**
1	0.6435	0.5793	0.5624	0.5563
3	0.8179	0.7363	0.7148	0.7071
5	0.8734	0.7863	0.7633	0.7550
7	0.9010	0.8111	0.7873	0.7788

Table 3.8: Sherwood Number when t=0.5.

Sc↓Kr→	**Sh**			
	1	**3**	**5**	**7**
0.22	0.5472	0.8283	1.0529	1.2422
0.6	0.9037	1.3678	1.7389	2.0513
0.78	1.0303	1.5596	1.9826	2.3389
1	1.1666	1.7659	2.2449	2.6483

Table 3.9: Sherwood Number when Sc=0.22.

Kr↓t→	**Sh**			
	0.5	**1**	**1.5**	**2**
1	0.5472	0.4926	0.4782	0.4730
3	0.8283	0.8140	0.8126	0.8124
5	1.0529	1.0490	1.0488	1.0488
7	1.2422	1.2410	1.2410	1.2410

Figures

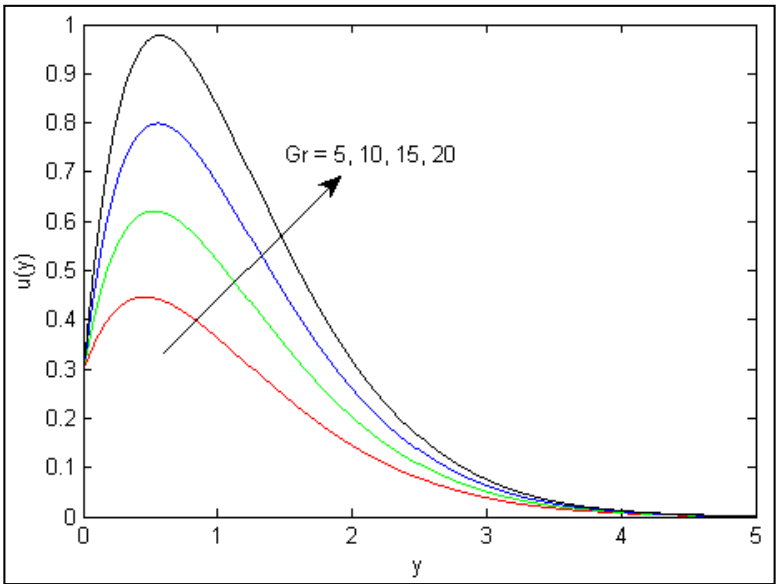

Fig 3.2: Velocity u against y for Gm=5, M=10, Kr=1, Pr=0.71, Sc=0.22, N=1, K_1=1, Q=1, α=1, t=0.3.

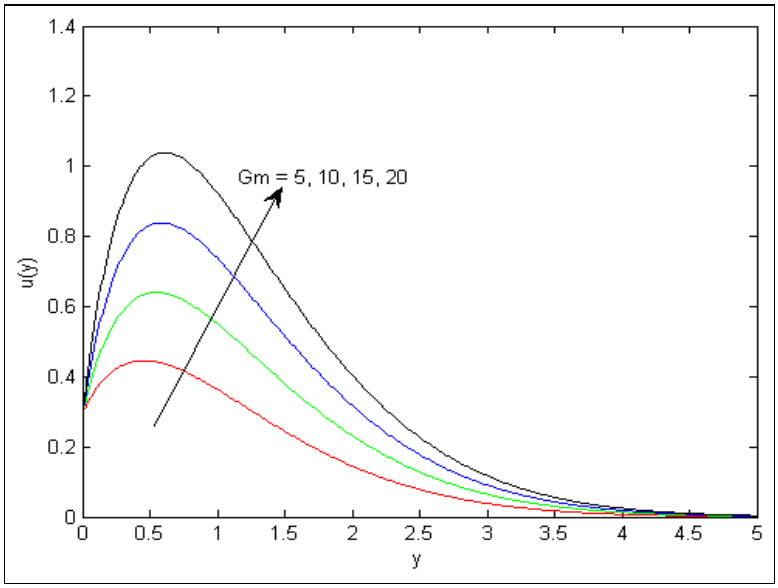

Fig 3.3: Velocity u against y for Gr=5, M=10, Kr=1, Pr=0.71, Sc=0.22, N=1, K_1=1, Q=1, α=1, t=0.3.

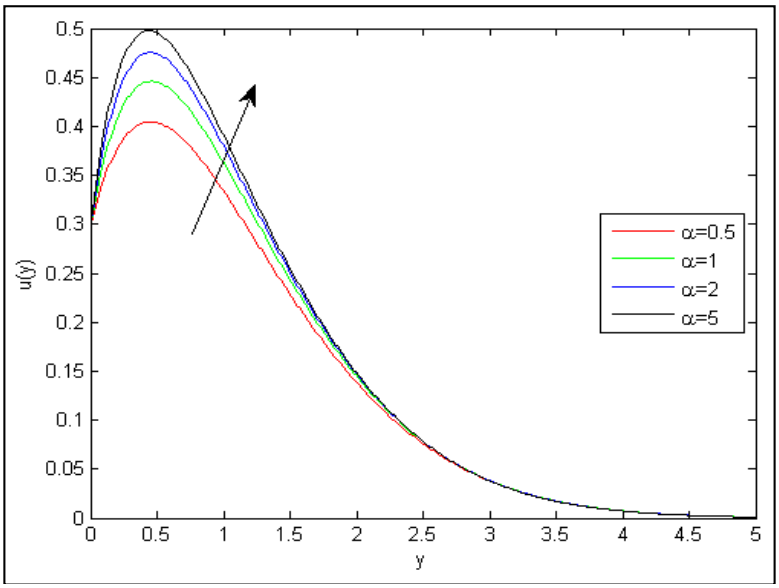

Fig 3.4: Velocity u against y for Gr=5, Gm=5, M=10, Pr=0.71, Sc=0.22, Kr=1, N=1, K_1=1, Q=1, t=0.3.

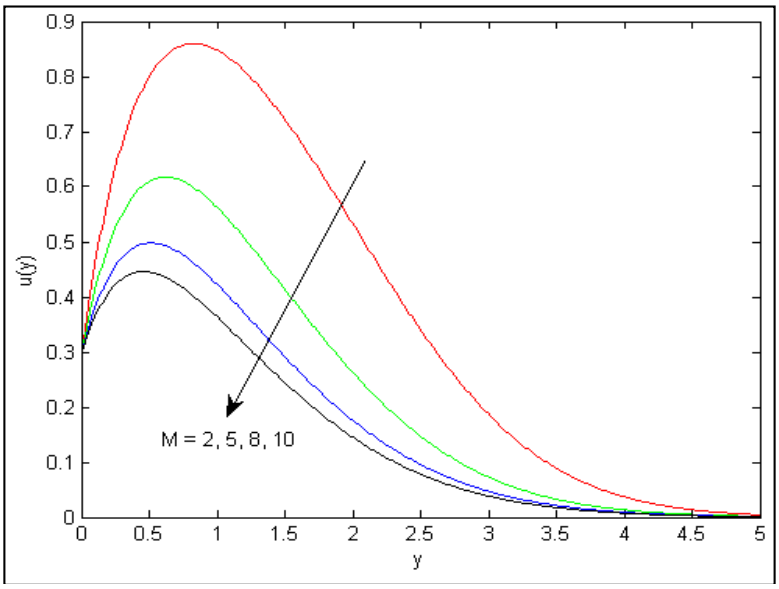

Fig 3.5: Velocity u against y for Gr=5, Gm=5, α=1, Pr=0.71, Sc=0.22, Kr=1, N=1, K_1=1, Q=1, t=0.3.

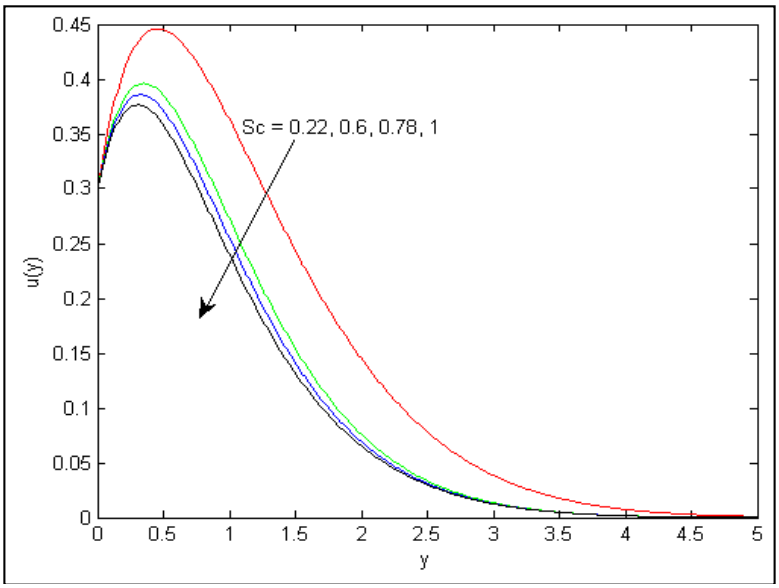

Fig 3.6: Velocity u against y for Gr=5, Gm=5, M=10, Pr=0.71, Kr=1, N=1, K_1=1, α=1, Q=1, t=0.3.

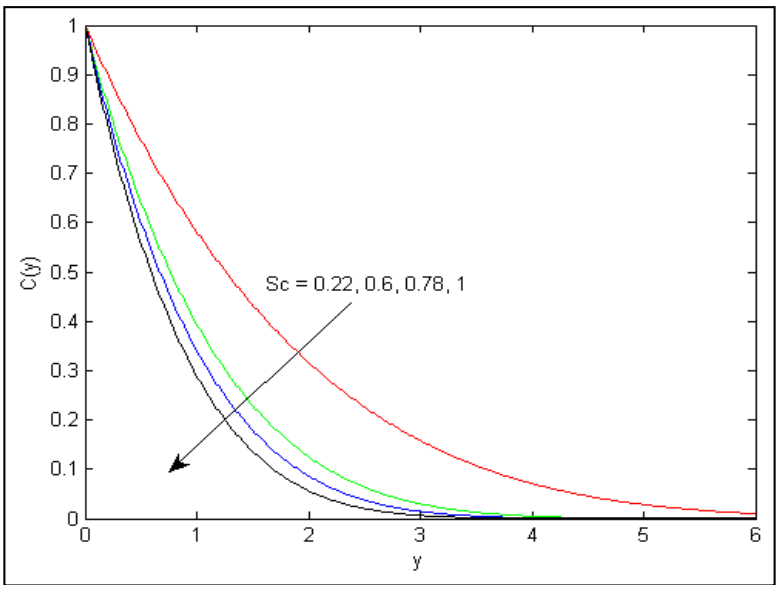

Fig 3.7: Species Concentration C against y for Kr=0.71, t=0.7

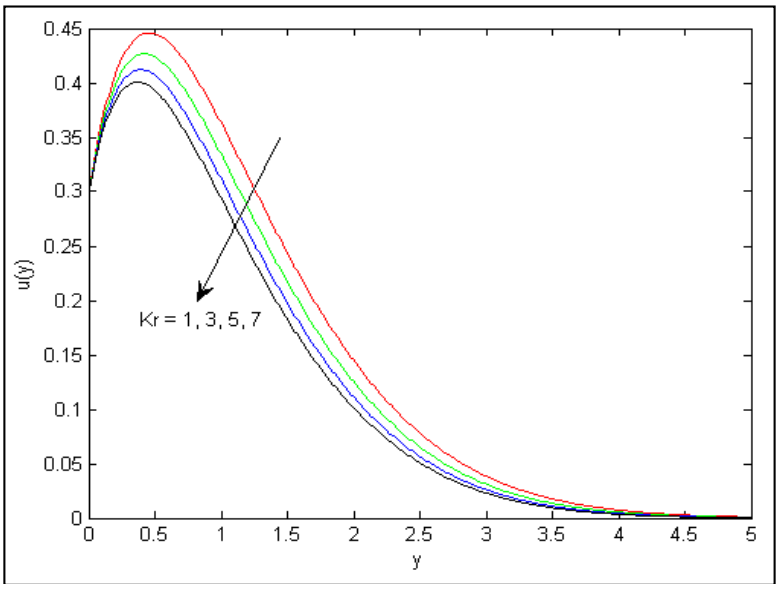

Fig 3.8: Velocity u against y for Gr=5, Gm=5, M=10, Pr=0.71, Sc=0.22, N=1, K_1=1, α=1, Q=1, t=0.3.

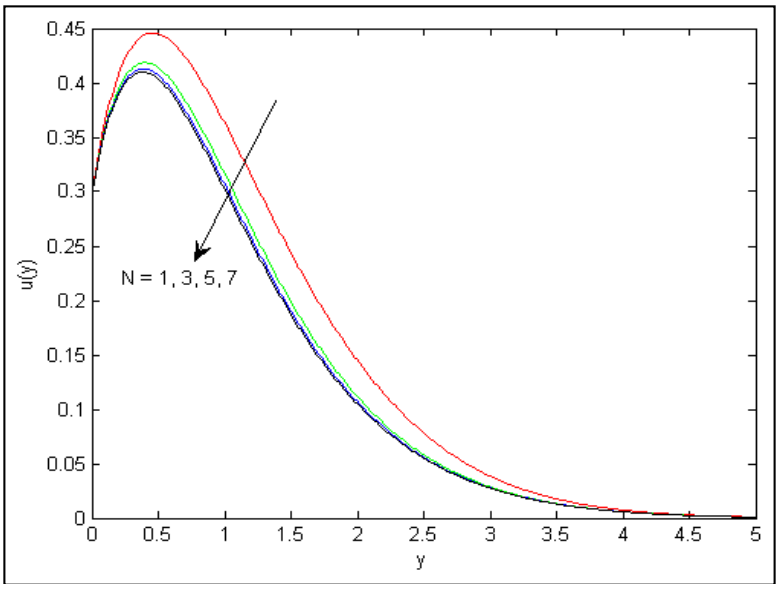

Fig 3.9: Velocity u against y for Gr=5, Gm=5, M=10, Pr=0.71, Sc=0.22, Kr=1, K_1=1, α=1, Q=1, t=0.3.

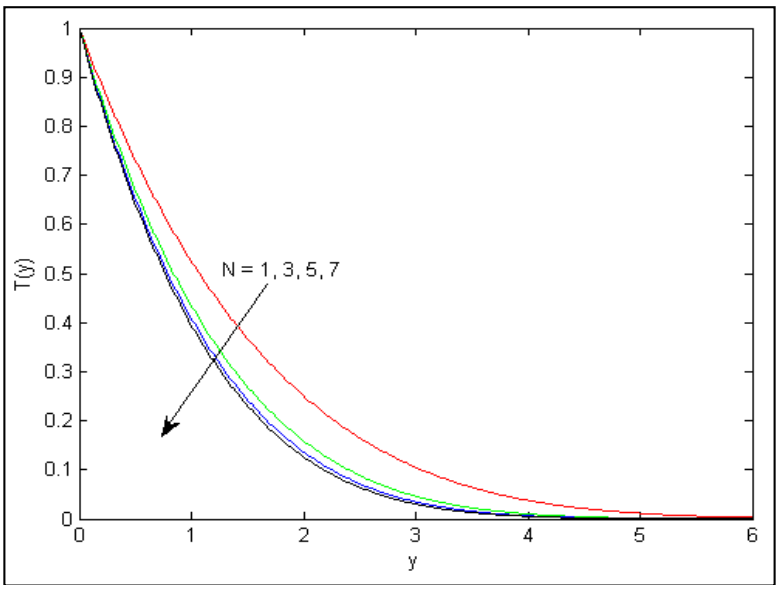

Fig 3.10: Temperature T against y for Pr=0.71, Q=1, t=0.7

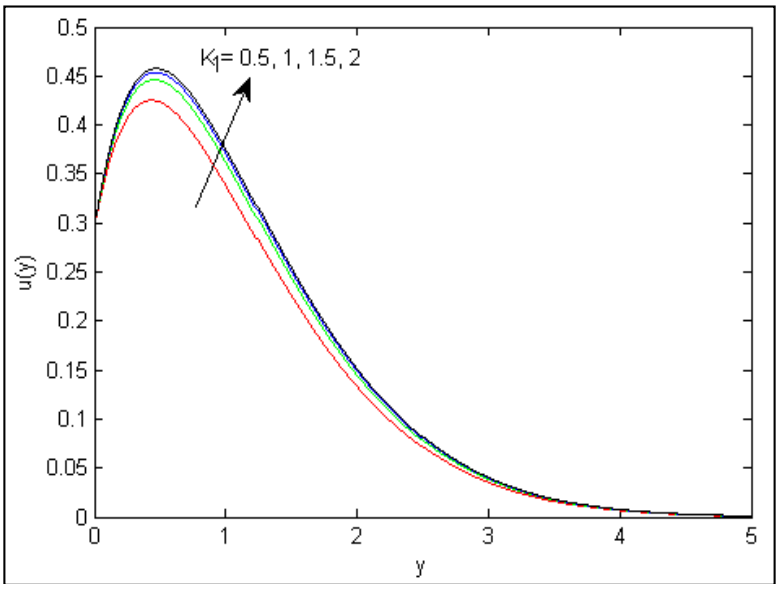

Fig 3.11: Velocity u against y for Gr=5, Gm=5, M=10, Pr=0.71, Sc=0.22, Kr=1, N=1, α=1, Q=1, t=0.3.

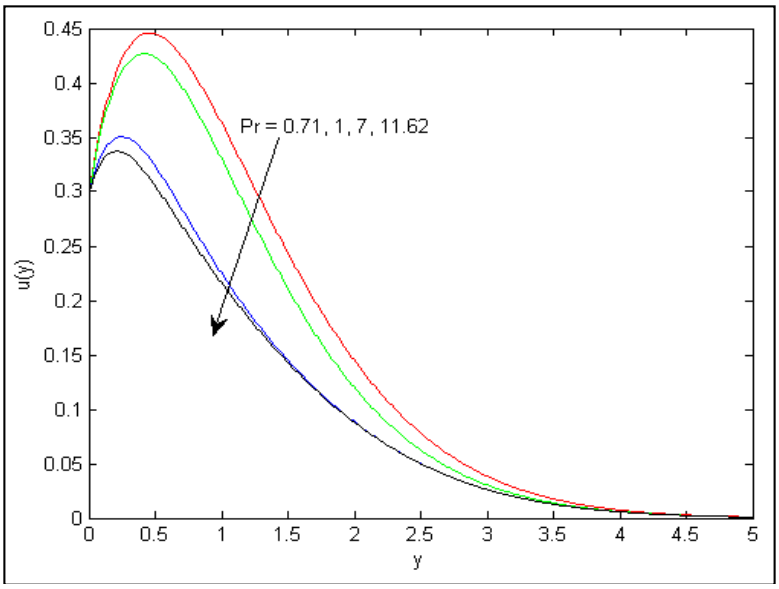

Fig 3.12: Velocity u against y for Gr=5, Gm=5, M=10, Sc=0.22, Kr=1, N=1, K_1=1, α=1, Q=1, t=0.3.

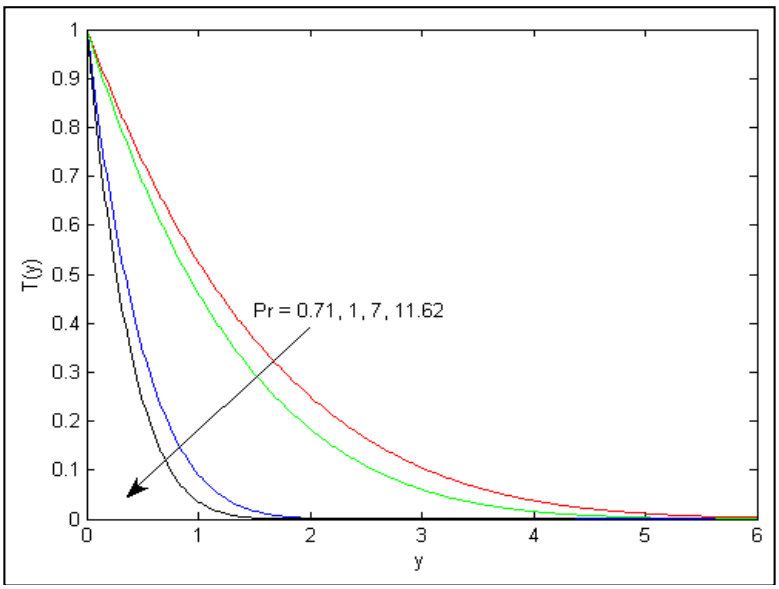

Fig 3.13: Temperature T against y for N=1, Q=1, t=0.3

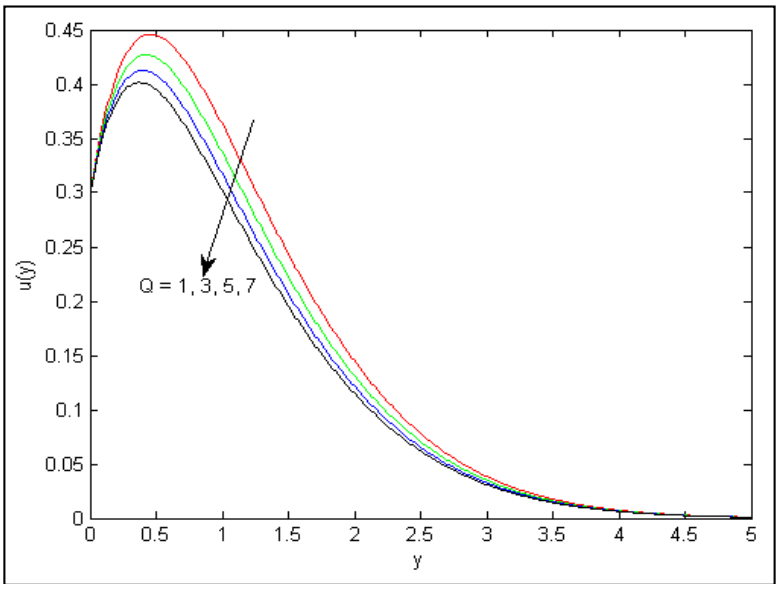

Fig 3.14: Velocity u against y for Gr=5, Gm=5, M=10, Pr=0.71, Sc=0.22, Kr=1, N=1, K_1=1, α=1, t=0.3.

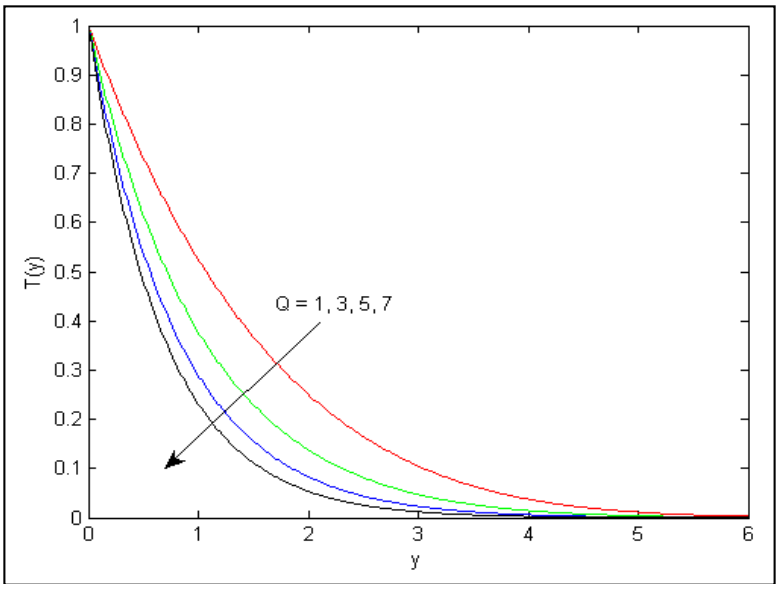

Fig.3.15: Temperature T against y for Pr=0.71, N=1, t=0.3

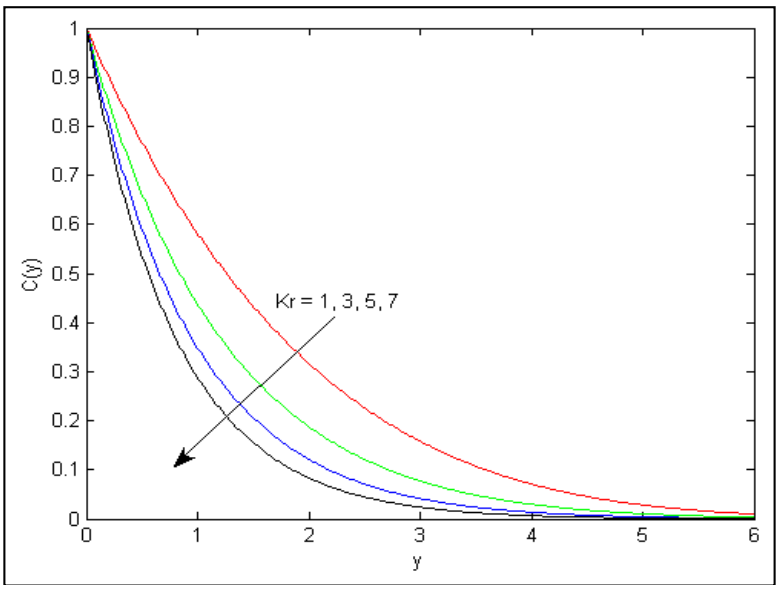

Fig 3.16: Species Concentration C against y for Sc=0.22, t=0.3

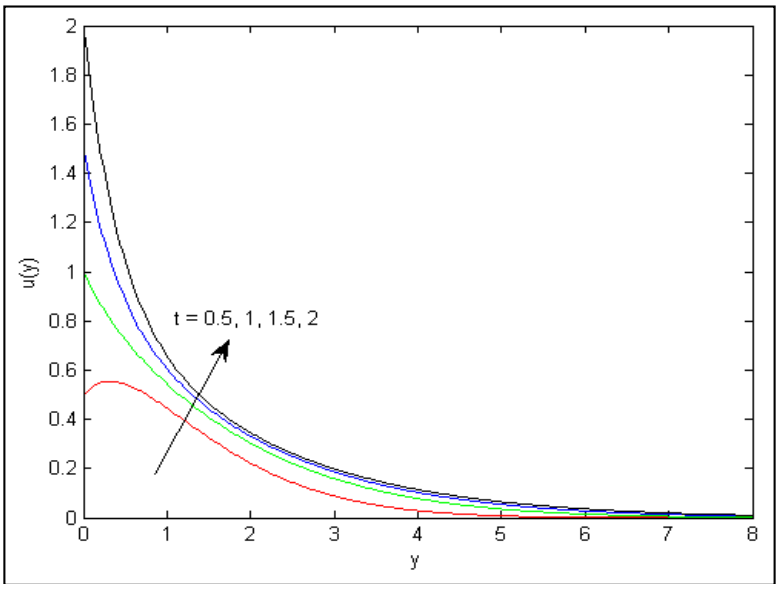

Fig 3.17: Velocity u against y for Gr=5, Gm=5, M=10, Pr=0.71, Sc=0.22, Kr=1, N=1, K_1=1, α=1, Q=1.

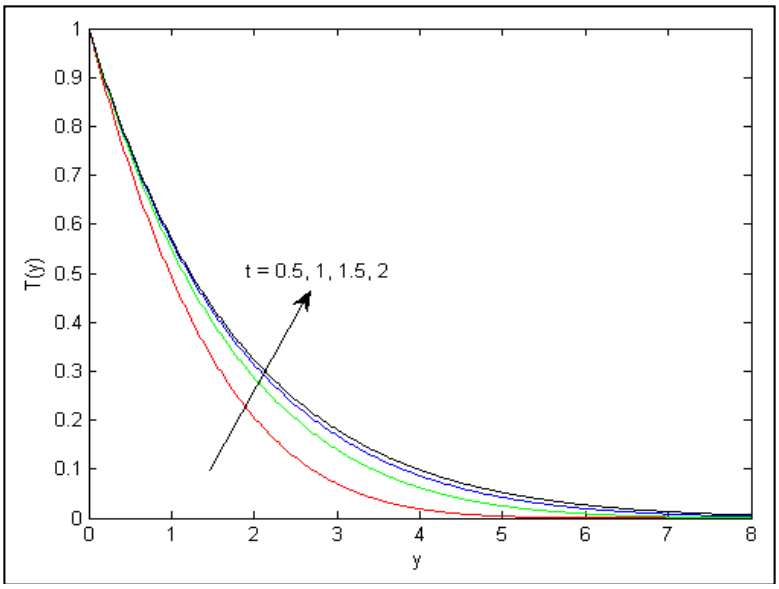

Fig 3.18: Temperature T against y for Pr=0.71, N=1, Q=1.

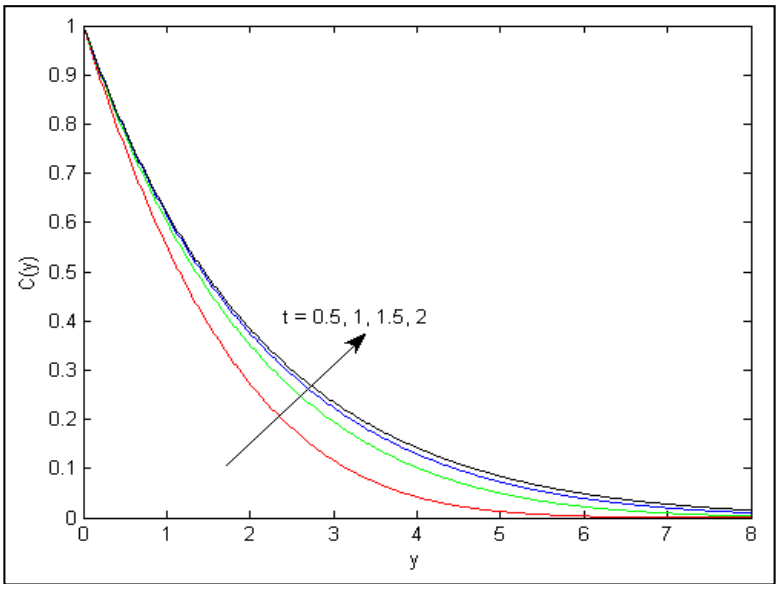

Fig 3.19: Species Concentration C against y for Kr=0.71, Sc=0.22.

Appendix $A_1 = 1 + \frac{1}{\alpha}, A_2 = M + \frac{1}{K_1}, A_3 = A_1 \frac{Pr}{\lambda} - 1, A_4 = A_2 - \frac{A_1 Pr Q}{\lambda}, A_5 = A_1 Sc - 1, A_6 = A_2 - A_1 ScKr,$

$A_7 = \frac{A_4}{A_3}, A_8 = \frac{A_6}{A_5}, A_9 = \frac{Gr}{A_3 A_7}, A_{10} = \frac{Gm}{A_5 A_8}.$

References

1. Vajervelue K, Shastri KS. "Natural convection heat transfer in vertical wavy channels", Int. J Heat Mass Transfer. 1980; 23:408-411.
2. Rajsekhar K, Raman Reddy GV, Prasad BDCN. Unsteady MHD free convective flow past a semi-infinite vertical porous plate, Int. J of Modern Eng. Research. 2012; 2(5):3123-3127.
3. Jefferey GB. The two dimensional steady motion of a viscous fluid, Phil. Mag. 1915; 29:455-465.
4. Lekoudis SG, Nayfeh AH, Sarie WS. Compressible boundary layers over wavy walls, Phys. of Fluids. 1976; 19:514-519.
5. Vajervelue K, Shastri KS. Free convective heat transfer problems between a long vertical wavy wall and a parallel flat wall, J. Fluid Mech. 1978; 86:365.
6. Shankar PN, Sinha UN. The Rayleigh problem for a wavy wall, J Fluid ech. 1976; 77:243-256.
7. Lesson M, Gangwati ST. Effect of small amplitude wall waviness upon the stability of the boundary layers, Phys. Fluids. 1976; 19:510-513.
8. Rao CNB, Sastri KS. The response of skin friction, wall heat transfer and pressure drop to wall waviness in the presence of buoyancy, Indian J Maths and Math. Sci. 1982; 5(3):585-594.
9. Ahmadi G, Mani R. Equation of motion for a viscous flow through a rigid porous medium, Indian J Tech. 1971; 9:441-452.
10. Rucha Luiz. Convection in channels and porous media", VDM Verlag.
11. Kundu KP, Cohen MI. Fluid Mechanics, Academic Press.
12. Schaat SA, Chambre PL. Flow of ……, Princeton Press, 1961.
13. Yamamoto K, Lwamura N. Flow with convective acceleration through a porous medium, J Eng. Math. 1976; 10:41-54.
14. Zarrouk SJ. Reacting flows in porous media, VDM Verlag.